Dual reconfigurable network from a semi-crystalline functional polyolefin

Diego Ciardi, Benedetta Rigatelli, Emmanuel Richaud, Michel Cloitre, François Tournilhac

▶ **To cite this version:**

Diego Ciardi, Benedetta Rigatelli, Emmanuel Richaud, Michel Cloitre, François Tournilhac. Dual reconfigurable network from a semi-crystalline functional polyolefin. Polymer, 2024, 297, pp.126864. ⟨10.1016/j.polymer.2024.126864⟩. ⟨hal-04560377⟩

HAL Id: hal-04560377

https://hal.science/hal-04560377v1

Submitted on 26 Apr 2024

HAL is a multi-disciplinary open access archive for the deposit and dissemination of scientific research documents, whether they are published or not. The documents may come from teaching and research institutions in France or abroad, or from public or private research centers.

L'archive ouverte pluridisciplinaire **HAL**, est destinée au dépôt et à la diffusion de documents scientifiques de niveau recherche, publiés ou non, émanant des établissements d'enseignement et de recherche français ou étrangers, des laboratoires publics ou privés.

HAL Authorization

Dual reconfigurable network from a semi-crystalline functional polyolefin

Diego Ciardi [a], Benedetta Rigatelli[b], Emmanuel Richaud[c], Michel Cloitre[a], François Tournilhac[a,]*

[a] Chimie Moléculaire, Macromoléculaire, et Matériaux, CNRS, UMR 7167, ESPCI−Paris, PSL Research University, 10 Rue Vauquelin, 75005 Paris, France.

[b] Université Lyon 1, CNRS, Ingénierie des Materiaux Polymères, UMR 5223, Lyon F-69003, France.

[c] Laboratoire PIMM, Arts et Metiers Institute of Technology, CNRS Cnam, HESAM Université, 151 boulevard de l'Hôpital, Paris 75013, France

Email: francois.tournilhac@espci.fr

Keywords: semi-crystalline, vitrimers, disulfides exchange, shape-memory

ABSTRACT :

A statistical copolymer p(E-co-GMA) of ethylene and glycidyle methacrylate (4.5 wt%) is considered as a starting point towards semicrystalline networks with exchangeable links. Application of the binomial law to size exclusion chromatographic data suggests that chains deprived of reactive comonomers would represent less than 6 wt% of the total, allowing to expect the formation of high gel-content networks. Experimentally, up to 98 wt% gel is obtained upon modification with 3,3'-dithiopropionic acid (DTPA). The crosslinking reaction can be performed in the molten state through a 2-steps procedure: 1°) x mol. of a commercial grade p(E-co-GMA), y mol. of DTPA and z mol. of triazabicyclodecene (TBD) are sheared in a twin-screw compounder at 115°C, a temperature right above the melting point of the polymer precursor, without triggerring the epoxy-acid addition; 2°) the thermolatent reactive blend thereby obtained is then crosslinked at 170°C. Samples with x = 1, y = 1 to 4 and z = 0 to 0.8 were thus prepared and evaluated. The presence of TBD accelerates disulfide exchange reaction, possibly by involvement of the thiolate anion whereas it decelerates the epoxy-acid addition. The final networks present several characteristic properties of vitrimers such as insolubility in xylene above the melting point, thermo-activated stress relaxation and creep. Particular shape memory regimes, related to the semicrystalline vitrimer character and the high insoluble fraction are demonstrated. Eventually, production scale-up using continuous reactive extrusion is evaluated.

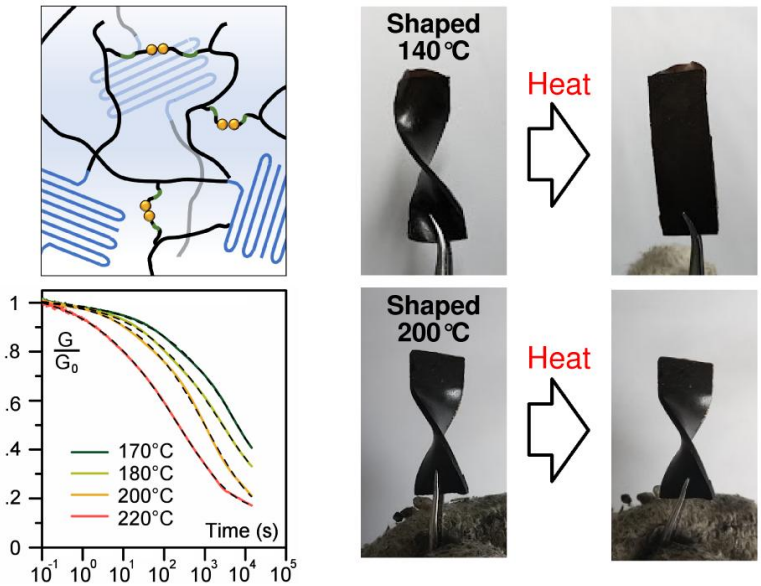

1. Introduction

Modifying existing polymers using reactive extrusion provides an attractive approach to synthesize new copolymer materials with tunable additional functionalities and morphologies. [1,2]. The fact that all reactions are performed in the melt, without addition / removal of solvent or by-products makes these processes easily scalable to continuous extrusion techniques. In this context, addition reactions represent a particularly favorable case in that formation of a new bond does not result in release of water or any other molecule [3]. Among possible modifications, transformation of a linear polymer into a branched or cross-linked polymer is an operation which can turn to be interesting insofar as it can improve the usage properties in a temperature range where the pristine thermoplastics tends to flow [4]. It is nevertheless against nature to do it by extrusion since the polymer no longer flows once crosslinked and therefore is no longer extrudable.

A possible exception to this rule is the case of vitrimers. Despite being crosslinked, vitrimers remain flowable due to the involvement of thermoactivated exchange reactions [5]. Production of vitrimers by reactive extrusion has been reported several times [6,7,8,9,10,11]. Nevertheless, the operation remains delicate because the introduction of exchangeable links considerably increases the melt viscosity, typically ranging from 10^2–10^4 Pa·s for the molten pristine polymer to 10^6–10^8 Pa·s for the vitrimer [6].

In the case of polyolefin vitrimers, it has been observed that the flow behaviour of a cross-linked polyethylene with exchangeable bonds largely depends on the presence of a soluble fraction, which does not participate in the network and imparts a flow behaviour to the vitrimer, which more closely resembles that of a thermoplastic polymer [12]. However, for materials with a higher gel content and greater homogeneity, extrusion can become more challenging, since no soluble fraction can act as a lubricant for the rest of the network.

One way to proceed is to limit the time spent in the extruder to the sole operation of mixing and to carry out the actual crosslinking ex-situ, for example through a curing step after injection. This strategy where the material is extruded in a thermolatent reactive state, called a pre-vitrimer, has been successfully applied to continuous extrusion of a polyester based vitrimer where the branching reactions inside the extruder were limited to below the gel point [13].

In this work, we investigate polyethylene-based vitrimers whose ability to relax stress entirely depends on the rearrangement of the network involving exchangeable disulfide bonds, since almost no soluble fraction is detected in the network. Disulfide functions have already been implemented in different systems, such as polyether elastomers [14,15] poly(urea-urethanes)

[16], epoxy resins [17,18] and proved to be activable by different stimuli including photoirradiation [19], mechanical stress [20], or heat.

The system hereby investigated consists of a statistical copolymer p(E-co-GMA) of ethylene and glycidyl methacrylate, which is transformed into a network using dithiodipropionic acid, HOOC−$(CH_2)_2$−S−S−$(CH_2)_2$−COOH as a crosslinker. The epoxy-acid addition between the polymer epoxide groups and the carboxylic acid functions of the cross-linker molecules leads to the formation of β-hydroxyl links, which are potentially exchangeable by trans-esterification reactions [5]. The disulfide bonds thereby introduced constitute another type of exchangeable bonds [21]. The combination of transesterification and disulfide exchange reactions has previously been explored in other works involving epoxidized natural rubber [21] and epoxy vitrimers [22], which highlighted the potential to enhance the stress-relaxation behaviour of networks compared to using only one type of bond. Here we demonstrate that, by careful design of catalytic and operating conditions, epoxy-acid addition can be accelerated or slowed down and the system can be maintained in a thermolatent reactive state throughout the extrusion process. A catalytic effect is also considered for the exchange reactions, as both transesterification [23] and disulfide exchange [24] are accelerated by basic organocatalysts. Despite being fully crosslinked, the resulting material remains reshapable, as demonstrated by stress-relaxation and erasable shape-memory properties. Furthermore, the effect of topological rearrangement on crystal orientation and its interplay with shape-memory effect will be discussed.

2. Experimental

2.1 Materials

Polyethylene-co-glycidyl methacrylate, p(E-co-GMA) was obtained from SK functional polymers. The commercial grade used (Lotader® AX8840) has target values of 4.5 wt% glycidyl methacrylate, melt flow index (190°C / 2.16 kg) of 5 g /10 min and density ρ = 0.93 g/cm^3. The cross-linker 3,3'-dithiodipropionic acid (DTPA, 99 %) and catalyst 1,5,7-triazabicyclo[4.4.0]dec-5-ene (TBD, > 98 %) were obtained from TCI; palmitic acid (99%) was obtained from Aldrich. Blending was achieved using a DACA twin-screw mini compounder operating at 300 rpm screw rotation speed. For each sample, 3 g of p(E-co-GMA) was introduced together with the required quantity of DTPA and TBD at 115 °C and mixed for 10 min. Alternatively continuous extrusion was performed using a Rondol "All-in-One" vertical twin screw extruder. In this case, pellets of p(E-co-GMA) were cooled at low temperature with liquid nitrogen and grinded into a powder. DTPA and TBD were mixed in

the molten state at 160°C, then cooled down to a solid which was further on pulverized in a mortar. The two powders were finally mixed together and introduced into the extruder through the upper feeding zone of the column.

2.2 Gel permeation chromatography (GPC)

GPC analyses were performed using an Agilent HT 220 system equipped with a refractive index (RI) detector in 1,2,4-trichlorobenzene (TCB) stabilized with 0.0125% BHT at 135 °C as mobile phase with two PLgel Olexis columns (Agilent Technology) as stationary phases. P(E-co-GMA) was dissolved in TCB (about 3 $g \cdot L^{-1}$). The elution method consisted in an isocratic step at 1 $mL \cdot min^{-1}$ flow of TCB for 30 min at 135°C. The calibration was done with polystyrene (PS) standards. Molar masses of p(E-co-GMA) were then estimated using universal calibration, by considering the Mark-Houwink parameters for PS ($K_{PS} = 14.1 \times 10^5$ $dg \cdot L^{-1}$; $\alpha_{PS} = 0.7$) and for PE ($K_{PE} = 95.4 \times 10^5$ $dg \cdot L^{-1}$; $\alpha_{PE} = 0.640$).

2.3 Nuclear magnetic resonance (NMR)

The microstructure of the polymer precursor was analysed using ^1H NMR spectra recorded in TCE/C_6D_6 mixture (volume ratio 2/1) at 363K on Bruker spectrometers working at 400 MHz. The solutions were prepared at 1-2% (w/v) and 1D-^1H spectra were recorded with a 5 mm BBFO+ probe equipped with a z-gradient coil. Chemical shift δ values are given in parts per million (ppm) with the solvent peak as internal standard.

2.4 Infrared spectroscopy

The cure monitoring was performed by infrared spectrometry in the 4000 – 600 cm^{-1} spectral range. Thin samples (thickness of about 40-60 μm) were prepared by compressing about 40 mg of extruded material between two silicon paper sheets under a weight of 2 tons (2 minutes at 115°C). Spectra were recorded in transmission using a Bruker Tensor 37 spectrometer equipped with a Specac 5750 heating jacket. The sample was placed between ZnS optically polished windows, previously heated to let the polymer stick on the surface. The cell, isolated by two external ZnS windows was flushed with argon. In-situ monitoring of chemical reactions was carried out at 4 cm^{-1} resolution. Before each series of experiments, a background spectrum was taken at the relevant temperature with all windows mounted but no sample present.

2.5 Thermal analysis

Thermogravimetric analysis (TGA) is described in the Appendix. Mechanical tests at low strain were performed using a Q800 DMA (TA Instrument, USA) operating in tensile mode on rectangular samples with dimensions of $35 \times 5 \times 1.5$ mm (nominal length ≈ 15 mm), at a frequency of 1 Hz and with a heating regime of -115°C to 180°C at 3°C/min. The cross-linking density ν_x and average molar mass per cross-link M_x of the polymer networks were then estimated using equation (1):

$$\frac{E'}{3RT} = \nu_x = \frac{\rho}{M_x} \qquad (1)$$

where ρ is the density in the molten state, taken equal to ρ_{150} = 0.80 g/cm^3 at 150°C [25], T the temperature, R the perfect gas constant and E' the value of the dynamic storage modulus at 150°C, as measured by DMA.

2.6 Swelling tests

Swelling tests were performed in xylene at 125°C. About 0.2 g (m_i) of sample was placed in a round-bottom flask equipped with a reflux condensor. After 12h, the solid residue was collected and weighed (m_s), then dried in a vacuum bell at 140°C for 12h. The mass of the dried specimen (m_d) was finally registered. The swelling ratio (Q) and the gel content (G) (both expressed in wt%) were evaluated according to equations (2) and (3):

$$Q = 100\,\frac{m_s - m_d}{m_s} \qquad (2)$$

$$G = 100\,\frac{m_d}{m_i} \qquad (3)$$

2.7 Shape memory and reshaping ability

Q800 DMA was used to quantitatively assess the shape memory behaviour of semi-crystalline networks with exchangeable bonds. A rectangular specimen with dimensions of about 35 mm × 7.4 mm × 1.5 mm was placed between DMA clamps in tensile mode. Shape memory behaviour was characterized using the four-step protocol A. Step A1: the sample is annealed during 5 min at 140°C. Step A2: the rectangular shape is elongated by applying a tensile stress of 100 kPa at 140°C. Step A3: a cooling ramp of -5°C/min is applied down to 20°C, while keeping the stress applied. Step A4: external stress is removed and the sample is re-heated to 140°C at 10°C/min. Deformation is measured throughout the different steps to

determine shape fixity and shape recovery, as usually defined [26]. Shape memory behaviour was further characterized on a second sample using the four-step protocol B, featuring different annealing time and temperature: Step B1: the sample is annealed during 35 min at 200°C. Step B2: the rectangular shape is elongated by applying a tensile stress of 100 kPa at 200°C. Step B3: a cooling ramp of 3°C/min is applied down to 20°C, while keeping the stress applied. Step B4: external stress is removed and the sample is re-heated to 200°C at 3°C/min.

2.8 Rheological measurements

The sol-gel transition of the thermolatent blends was monitored by using an Anton Paar MCR501 rotational rheometer equipped with a 25mm parallel plate geometry. The materials here investigated have been first obtained by extrusion and compressed into a cylindrical shape using a stainless-steel mould (radius r = 25 mm, thickness 1.5 mm) at 115°C, applying a pressure of 3 tons on the moulds for 3 min. The upper and lower geometries are a stainless-steel plate and a disposal aluminium plate, respectively. To minimize thermal degradation, the plate geometry was enclosed in a convection oven under a 200L/h nitrogen flow. Before starting every experiment, the oven was preheated at 115°C, above the melting temperature of the pristine polymer, and the sample was placed onto the aluminium plate to ensure good contact. The upper geometry was the gradually lowered onto the sample for proper adhesion. The temperature was then raised to 170°C and kept constant for the rest of the experiment.

Linear viscoelastic properties of the cured samples were evaluated with a strain-controlled Ares-G2 (TA Instrument) rheometer operating in the torsion mode. Rectangular samples were shaped, with a dimension of about 50 × 16 × 5 mm. During all experiments, a tension force of 100 gram-force (≈ 0.98 N) was applied. Time sweep, amplitude sweep, frequency sweep and stress-relaxation experiments were performed. Time sweep was first carried out at 2% strain to assess the evolution of the storage, *G'*, and loss, *G''*, moduli over time at 170°C and 1 rad/s (Fig S5a, S6a). Experiments at different strain amplitudes were then performed at the same temperature to determine the linear regime (Fig S5b, S6b). Finally, frequency sweep and stress relaxation experiments were performed on fresh samples for each tested temperature, by applying a constant strain γ = 2%. Frequency sweeps experiments were performed between 100 rad/s and 0.1 rad/s, while stress relaxation experiments were monitored during up to 4h and then repeated on the same sample.

3. Results

3.1 Precursor copolymer characterization

The semi-crystalline precursor is a commercial statistical ethylene copolymer, p(E-co-GMA), with a nominal fraction of 4.5 wt.% (0.93 mol%) of glycidyl methacrylate (GMA) comonomers. These functional moieties are the reactive sites which will be used as cross-linking points for the formation of dynamic semi-crystalline networks. The effective concentration of the reactive monomer was first assessed by NMR (Fig. S1), which revealed 1.0 mol% of GMA, consistent with the nominal value. The polymer precursor thus presents 1 GMA unit every approximately 110 ethylene units, in average. The p(E-co-GMA) precursor was also analysed by GPC at 135°C in TCB. By applying the so-called universal calibration method based on the Mark-Houwink-Sakurada equation, the initially measured molar masses relative to PS standards have been converted into PE molar masses [27]. The result is reported in Fig. 1a, leading to M_n = 12 kg/mol, M_w = 99 kg/mol and Đ = 8.5. The polydispersity Đ obtained for p(E-co-GMA) indicates a wide distribution of polymer chain lengths. The number of reactive monomer GMA thus increases with the molar mass of the chain. Assuming random copolymerization of ethylene and GMA monomers, further analysis of the GPC signal using the binomial law [28] allowed to determine the respective weight fractions of polymer chains bearing a certain number N_x of GMA monomers. Such a weight distribution, plotted in Fig. 1b, was obtained by using equation (4):

$$\Phi\left(N, N_x\right) = \theta\left(N\right) \cdot \Psi\left(N, N_x\right) = \theta\left(N\right) \cdot \frac{N!}{(N - N_x)!\, N_x!}\, p^{N_x} \cdot (1 - p)^{N - N_x} \qquad (4)$$

where N is the degree of polymerization of the chain considered and N_x the number of GMA comonomers, Φ is the number fraction of chains with N ethylene units and N_x GMA comonomers, θ is the molar mass distribution obtained from the GPC trace of p(E-co-GMA), Ψ is the binomial distribution and p the average molar fraction of GMA (p = 0.93 mol%). The product of the two distributions θ and Ψ provides an assessment of the statistical distribution of the reactive groups along the polymer backbone as a function of the chain length. By integrating the resulting distribution Φ over N, it is possible to obtain the weight distribution of chains bearing N_x GMA, regardless of their length. As it can be observed in Fig. 1b, about 5.5% of polymer chains bear no reactive comonomer and the maximum of the distribution is observed for chains with 1 GMA. Due to the elevated polydispersity of the commercial p(E-co-GMA), it is possible to find polymer chains with up to approximately 300 GMA (Fig. 1c). So, when forming a gel starting from this polymer precursor, all the chains bearing at least 1

GMA are potentially integrated into the network, contributing to a high gel content value. Here, up to 95% gel content can be expected.

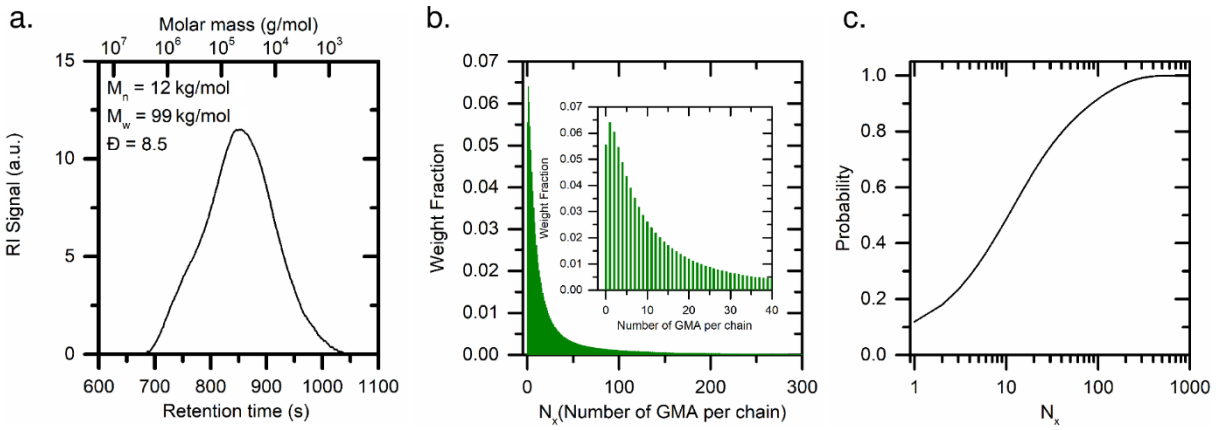

Fig. 1. (a) GPC trace of p(E-co-GMA); (b) Calculated weight fraction of chains bearing N_x reactive units per chain of the p(E-co-GMA) copolymer; (c) cumulative distribution function of the weight fraction distribution

3.2 Sample preparation

The compositions of the samples studied in the following are presented in Table 1. The preparation involves two steps as illustrated in Fig. 2. First, the polymer precursor p(E-co-GMA), the cross-linker DTPA and optionally the catalyst TBD are introduced into the twin-screw mini-compounder for 5 min, at 115°C. This preparation strategy allows to mix every component above the melting temperature T_m of the semi-crystalline polymer without triggering the epoxy-acid addition which would provoke cross-linking inside the machine. We call *pre-vitrimer* the thermolatent mixture thus obtained. In a second step, is the pre-vitrimer is cured for 1 to 7 h at 170°C in a mold of desired shape to obtain the chemically cross-linked network. Whereupon, the obtained compound is cooled down to room temperature causing a partial crystallization of the polyethylene phase, which forms a second, physical, network interpenetrated with the chemical network previously formed. The chemical cross-links formed during the second step contain hydroxy-ester and disulfide bonds which are prone to undergo thermally activated exchange reactions. We anticipate that the chemical network thus obtained is a vitrimer. The whole material therefore combines physically and chemically exchangeable networks; in the following it will be referred to as a *dual reconfigurable network.*

Table 1: Feed ratios and stoichiometry of samples prepared by reactive blending from the polymer precursor (pE-co-GMA), cross-linker (DTPA) and catalyst (TBD).

Compound	p(E-co-GMA) (g)	DTPA (g)	TBD (g)	Epoxy (eq)	COOH (eq)	TBD (eq)[a]
PE-1:1-0	3	0.1	0	1	1	0
PE-1:1-0.2	3	0.1	0.026	1	1	0.2
PE-1:4-0	3	0.4	0	1	4	0
PE-1:4-0.2	3	0.4	0.026	1	4	0.2
PE-1:4-0.8	3	0.4	0.104	1	4	0.8

[a] TBD equivalents are expressed relatively to the number of epoxy functions.

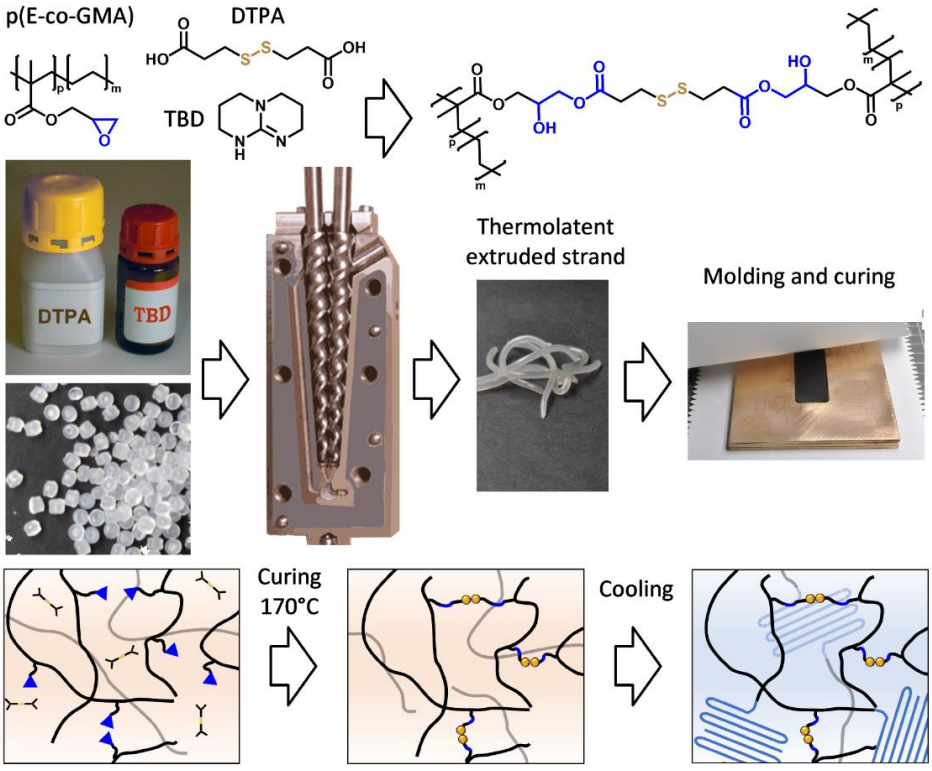

Fig. 2. Top: chemical structure of the p(E-co-GMA) copolymer, DTPA cross-linker, TBD catalyst and the resulting cross-linked polymer chains. Middle: workflow of samples preparation. Bottom: schematic illustration of networks' structure.

3.3 Reactive extrusion and curing

Immediately following extrusion, the materials are turbid. Those containing TBD appear brown, whereas those only containing the cross-linker remain colourless. At 170°C, while the precursor copolymer (pE-co-GMA) has a complex shear viscosity of 4000 Pa·s at 1 rad/s, the extruded compositions listed in Table 1 have viscosities still comprised in a range from η^* = 5000 to 9000 Pa·s i.e. not much higher. Meanwhile, IR analysis of all samples (Fig. S2) reveal the persistence of the characteristic epoxy band at about 914 cm^{-1} with almost unchanged intensity. These facts confirm that the compositions at this stage are pre-vitrimers that are still reactive and not yet cross-linked.

The curing reaction of the pre-vitrimers was followed by IR spectroscopy and rheology at 170°C (Fig. 3). The time dependence of the epoxy IR signal (at 914 cm^{-1}), normalized by its initial value measured in the pre-vitrimer state (Fig. S2) is plotted in Fig 3a. The decay of this signal demonstrates that full cure is achieved in about 1 to 6 h, depending on the composition. Meanwhile, the effective formation of crosslinks is detected by the sudden rise of viscosity upon approaching the gel point (Fig 3b).

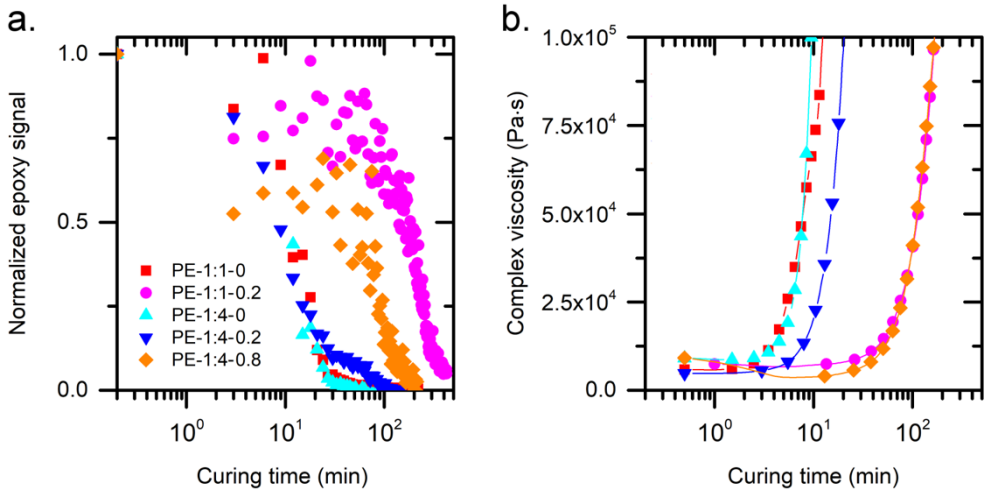

Fig. 3. Time dependence of chemical and mechanical signals during curing reaction at 170°C. a) Decay of the normalized IR epoxy signal (914 cm^{-1}). b) Rise of viscosity showing the onset of the gel point.

From IR kinetics in Fig. 3a, it is observed that the speed of disappearance of the epoxy signal depends on the composition. It is interesting to observe that when TBD is present the drop of the epoxy signal is slowed down. This effect is counter-intuitive since we expect a basic catalyst like TBD to lead to the formation of alkoxide anions, which are more basic than the

carboxylate anion, thus favouring transesterification, Fischer esterification and epoxide-hydroxylate reaction [29]. Specifically, TBD is known as a catalyst of ring opening reactions like homopolymerization of lactide [30]. In epoxy-acid systems, TBD was shown to equally catalyse the epoxy-acid addition and the epoxy homopolymerization, whereas a conventional imidazole catalyst clearly favored the former reaction [31]. It remains difficult to accurately follow the kinetics of all the chemical species of interest in our system, due to an overlapping of peaks related to the carbonyl vibration of the methacrylate moiety (1733 cm^{-1}) and the ester group (1725-1748 cm^{-1}) that is expected to form. Nevertheless, a global slow-down is observed in the presence of TBD. Alongside reasons attributable to different reactions involved, early works have pointed out how the base-catalysed epoxy-acid addition is hindered in apolar solvents due to the involvement of ammonium/carboxylate ion pairs intermediate, showing poor solubility in low dielectric constant media [32,33], which is also the case here. Another observation in line with such effects is that whenever a higher concentration of acid cross-linker is present for compounds PE-1:4-0.2 and PE-1:4-0.8, the reaction rate further decreases, confirming that the formation of epoxy/carboxylic/TBD complexes influences the reaction kinetics. A more precise insight into the possible side reactions occurring during gelation was revealed by monitoring the gelation of a blend of the polymer precursor with a monocarboxylic acid (palmitic acid) instead of the dicarboxylic cross-linker (Fig. S3). With palmitic acid, the epoxy-acid addition cannot lead to the formation of interchain links, nevertheless, a gel is formed for all the tested compositions, confirming that above mentioned secondary reactions take place. Furthermore, when a higher content of TBD is present, the gelation time is shifted to even longer values, thus indicating that TBD preferentially catalyses epoxy-acid addition over the formation of permanent bonds.

3.4 Gel content of cured compositions.

The results of swelling tests are reported in Table 2. Once cured, all samples show gel content values reaching up to ~ 98%, in good agreement with the above expected value (~ 95%) inferred from the GPC analysis. Only the sample PE-1:1-0.2 shows a gel content of ~ 64% and a higher swelling ratio, suggesting partial cleavage of the disulfide links in the presence of TBD resulting in a decrease in crosslinking density in this sample where the quantity of crosslinker is not more than stoichiometric. In all other cases, it appears that 4.5 wt% of GMA

of the polymer precursor is sufficient to obtain materials that have a negligible amount of soluble fraction, which can potentially lead to macro-phase separation of the non-linked chains in the network [28].

Table 2: elastic modulus *E'*, cross-linking density ν_x, average molecular weight between cross-links, M_x as from DMA (see section 2.5) and gel content and swelling ratio from swelling tests (see section 2.6) for the obtained networks.

Compound	*E'* at 150°C (MPa)	ν_x (mol/cm^3)	M_x (g/mol)	Gel content (wt%)	Swelling ratio (wt%)
PE-1:1-0	3.51	$3.3 \cdot 10^{-4}$	2400	97	330
PE-1:1-0.2	2.29	$2.2 \cdot 10^{-4}$	3700	64	1560
PE-1:4-0	3.25	$3.1 \cdot 10^{-4}$	2600	93	370
PE-1:4-0.2	3.41	$3.2 \cdot 10^{-4}$	2500	96	360
PE-1:4-0.8	3.29	$3.1 \cdot 10^{-4}$	2600	98	350

3.5 Elasticity of formed networks.

The results of the dynamic mechanical analysis are presented in Fig. 4 and the values of the elastic modulus *E'* above the glass transition are reported in Table 2. Different behaviours can be observed depending on the composition. First, in the temperature range between -40°C and 110°C, the elastic modulus *E'* for p(E-co-GMA) is larger, due to its greater degree of crystallinity. Moreover, *E'* decreases by several orders of magnitude in all the tested samples, and three main transitions can be determined. At ~6°C, a first peak appears in the loss factor measured for the cross-linked networks. At 67°C, the α transition of polyethylene is only evident for the polymer precursor. This transition depends on the crystallinity of the polymer, which is reduced upon crosslinking (see SI Figure S3, Table S1), and it tends to move towards lower temperatures for lower crystallinity samples [34]. *E'* keeps decreasing until the melting temperature T_m of the polymer is reached. At this temperature, the elastic properties of p(E-co-GMA) are no longer measured, whereas the cross-linked samples show a rubbery plateau, whose modulus depends on the composition. The cross-linking density ν_x and the average molecular weight between cross-links M_x are calculated from the rubbery plateau at 150°C, by assuming that the polymer networks is incompressible (Poisson's ratio equal to 0.5).

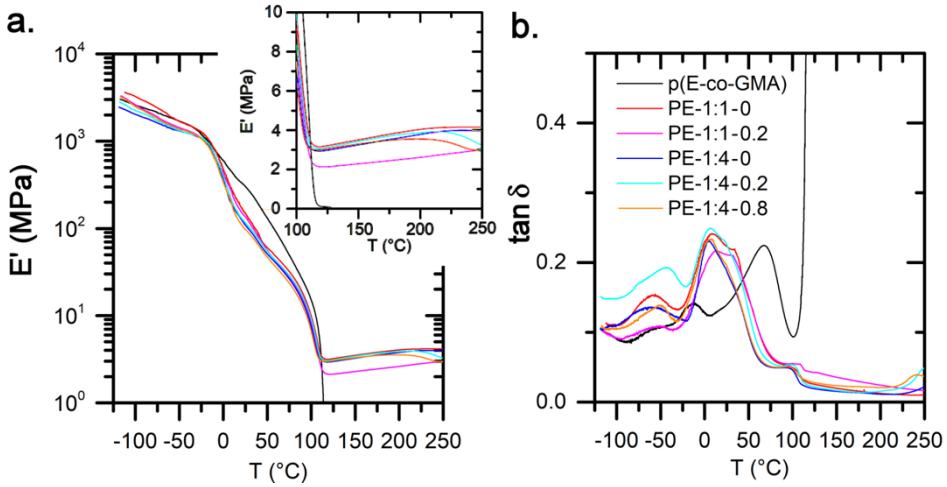

Fig. 4 Thermomechanical properties of the obtained networks at 1Hz: a) temperature dependence of the elastic modulus E'; b)the loss factor tan δ (right)

Based on the nominal fraction of GMA (0.93 mol%), the expected average mass between crosslinking points is of M_x = 3160 g/mol (weight of 107 ethylene + 1 GMA units). In Table 2, the measured values of M_x (from DMA), are in good agreement with the calculated one. This may indicate that each epoxy group has reacted with a carboxylic moiety, leading to a cross-linking point. However, when an excess of carboxyl group over epoxies is added, a fraction of crosslinkers should be bound to the polymeric backbone at one end only, thus decreasing the cross-linking density. This scenario would occur in case the epoxy-acid addition is the only reaction contributing to the formation of cross-links. We know instead that other reactions such as Fischer esterification, epoxy homopolymerization and ring opening polymerization can take place [31], making the network denser. Thus, for the majority of samples the rubbery modulus appears to be similar. Only for PE-1:1-0.2 we mesured a significantly smaller value, consistent with higher swelling ratio and lower insoluble fraction. The explanation for this result still lies in the multitude of mechanisms involved in network formation. As already discussed above and shown in Fig. S3, the formation of permanent ether bonds is reduced when a higher content of catalyst is present. In addition, the reduction of disulfides to thiols by a basic catalyst, already described in the literature [35], can also lead to the decrease of the cross-linking density and affect the elastic properties of the network. Such a reaction was shown to take place in the presence of amines as reducing agents, which deprotonate thiols to thiolates [36,37,38,39]. In amine-cured epoxy resins containing either aliphatic or aromatic disulfide bridges, a drop in initial shear modulus G_0 was observed at high temperature and attributed in both cases to bond dissociation [18],

albeit the effect was more pronounced in the aromatic case. For samples PE-1:4:0.2 and PE-1:4:0.8, a comparable drop is observed above 200°C for the storage modulus *E*' (Fig. 4a), showing that bond dissociations have to be taken into accounts in the exchange mechanisms.

3.5 Discussion about sulphur exchange mechanisms.

In addition to reducing the network connectivity, the reduction of disulfides to thiols can also influence exchange dynamics through the introduction of a secondary exchange mechanism [40,41,15,24]. When TBD is combined with DTPA, thiol and deprotonated thiolates can exchange with disulfide bonds via a three-step associative mechanism [20,38,42], in parallel with the radical-mediated mechanism generally described for disulfides [38,40,43]. Consequently, the overall network dynamics become faster, causing a drop in the *E'* modulus at high temperatures for PE-1:4-0.2 and PE-1:4-0.8 above 200°C in DMA. This observation is generally attributed to a cleavage of the reversible covalent bonds, leading to decrease of the network connectivity with temperature [18]. Therefore, in our systems, both radical and thiol/disulphide exchanges may take place. Since the drop in *E'* modulus is evident mainly for compounds PE-1:4:0.2 and PE-1:4:0.8, we believe that the thiolate/disulfide exchange becomes more important in these networks, especially due to the higher TBD content, which can catalyse thiol formation and exchange.

3.6 Vitrimer properties.

The rheological analysis of PE-1:4:0.2 is presented in Fig. 5; additional data for PE-1:4:0.2 and PE-1:4:0.8 are reported in Fig. S5 and S6. Frequency sweeps at different temperatures (Fig. 5a) show that PE-1:4:0.2 has a constant shear modulus *G'* over all the sampled frequency range, except at 220°C, where a slight drop in *G'* is observed at low frequency due to the exchange reaction, as already observed in DMA. More evidently, the loss modulus *G''* increases with temperature, indicating that the rearrangement of the network speeds up as the temperature is increased. At a given temperature, the change in slope of *G''* occurs at lower frequencies in the case of PE-1:4:0.8 (Fig. S5c), with a higher concentration of TBD, strengthening the hypothesis that the mechanism of the exchange reaction is controlled by the concentration of the catalyst, directly and indirectly through the involvement of thiolates [24]. In Fig. 5a and for all temperatures, the absence of cross-over between *G'* and *G''* at low frequency indicates the relaxation modes associated with the exchange of dynamic covalent bonds occur at longer times than those accessible using oscillatory measurements.

Stress relaxation experiments under a constant strain of γ = 2% were performed in order to access long time scales. The time dependant relaxation modulus $G(t)$ of PE-1:4:0.2 is plotted in Fig. 5b and 5c. The normalized relaxation modulus shown in Fig. 5c is fitted to a stretched exponential function to obtain the average relaxation time $\langle\tau\rangle$ at each temperature, according to equations (5) and (6).

$$G(t) = G_\infty + G_0 e^{-(t/\tau^*)^\beta} \qquad (5)$$

$$\langle\tau\rangle = \frac{\tau^*}{\beta}\Gamma\left(\frac{1}{\beta}\right) \qquad (6)$$

where G_∞ is the residual stress obtained from the fitting model, G_0 is the pre-exponential factor, τ^* the relaxation time, β the relaxation exponent and Γ the gamma function. The values of G_∞, $\langle\tau\rangle$ and β are reported in Table 3. From the logarithmic plot of $\langle\tau\rangle$ as a function of 1/T, an activation energy is determined. Such plot for PE-1:4:0.2 is shown in Fig 5d, where the activation energy E_a is about 120 kJ/mol. The values obtained for β deviate from unity, indicating that the relaxation of the stress involves a distribution of relaxation times possibly reflecting the presence of several mechanisms and the broad size distribution of objects whose relaxation is observed. Indeed, both β-hydroxyl ester and disulfide species can contribute to exchange reactions, whereas permanent crosslinks broaden the size distribution of the polymer precursor. Interestingly, the obtained relaxation time values differ from those typically observed for disulfide-based vitrimers. While a wide range of activation energy values was extracted from stress-relaxation experiments for disulfide vitrimers [17,22,44,45] (ranging from 55 to over 300 kJ/mol), they have been observed to relax stress within a few seconds at high temperatures, even without the action of an external catalyst. We believe that the slower relaxation times of our system are related to the structure of the network, which is composed of long polyethylene (PE) chains and high gel fractions.

Indeed, disulfide-based vitrimers so far investigated generally consist of networks composed of small units (single molecules) linked to each other by exchangeable bonds. When two bonds exchange, small fragments of the network can interact with a nearby neighbour and locally relax. In contrast, in our case, the network is composed of long unbreakable PE chains. This means that an entire chain must reshuffle all the exchangeable bonds attached to it before moving and achieving a transport of matter within the network, which considerably delays the relaxation time.

At 220°C, the relaxation modulus $G(t)$ of PE-1:4-0.2 reaches a plateau value after 3000 s. This change in the slope of the stress-relaxation traces may be attributed to various factors,

including the presence of a second exchange mechanism between the cross-links. Indeed, in our case, the transesterification reaction can also occur and thus contribute to the overall relaxation of the network. As this exchange reaction is generally slower than the exchange between disulfides, it is likely to become evident over longer periods and only at higher temperatures. In addition, the slower relaxation at longer times can also be related to the presence of permanent bonds originating from secondary reactions such as homopolymerization or ring opening polymerization. Once the network is formed, non-exchangeable bonds limiting the capacity of the thiol/disulfide reaction to relax stress can also form upon the oxidation of thiols, as already observed in disulfide-based systems [46].

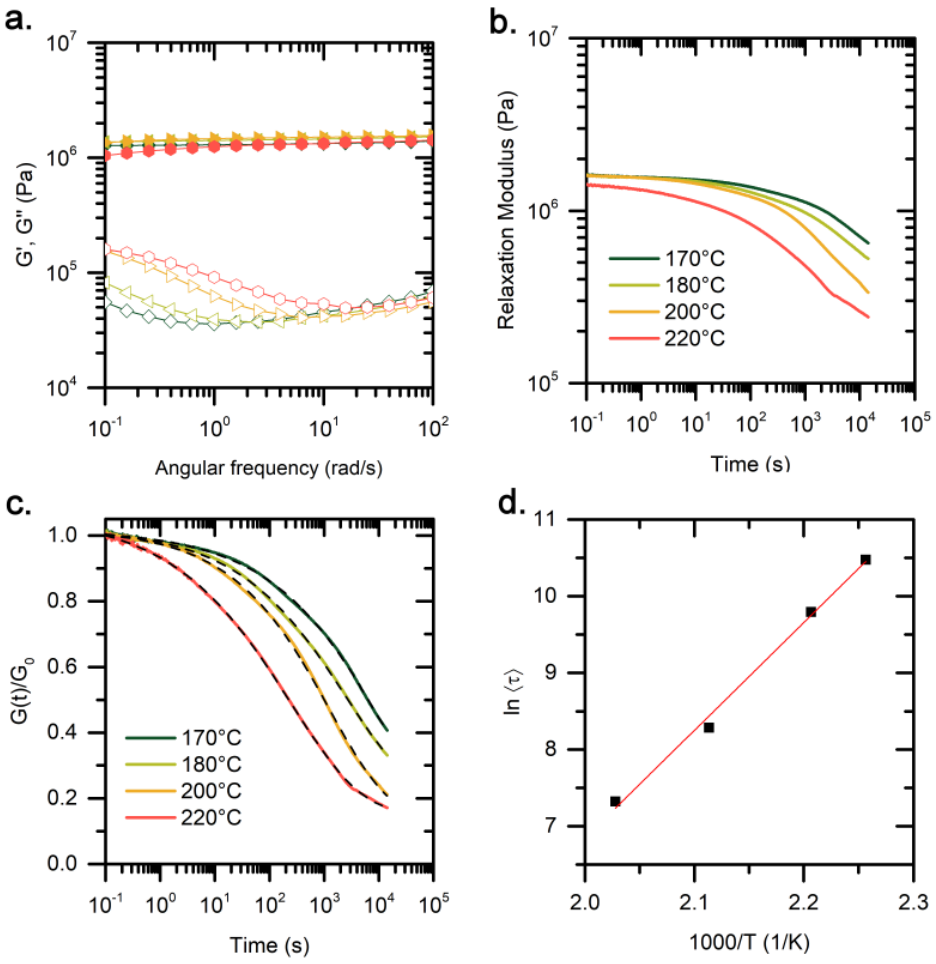

Fig. 5: linear viscoelastic properties of PE-1:4:0.2 between 170°C and 220°C. For each temperature, a fresh sample undergoes frequency sweep (a), first, and stress-relaxation (b) experiments. (c) Normalized relaxation modulus is fitted (dash line) to obtain the average relaxation time $\langle\tau\rangle$ and the activation energy E_a in (d).

This is further observed when a second stress relaxation experiments is performed on the same material: at all temperatures, the stress relaxation in the second experiment is slower than in the first one and the residual stress after 4h, $\sigma_{r,2}$ is larger than $\sigma_{r,1}$ (Fig. S5c, d). The

difference between $\sigma_{r,1}$ and $\sigma_{r,2}$ increases with the temperature. In addition, after the second stress-relaxation experiment, the relaxation curves cannot be fitted with the same stretched exponential model. In addition to the oxidation of thiols, a degradation of the catalyst can also occur when reaching too high temperatures (Fig. S7). For the sample PE-1:4:0.8, deviation of the stress-relaxation curves from the exponential model is already evident in the first experiment, suggesting that oxidation and/or degradation are more pronounced when a higher catalyst content is present (Fig. S5d).

Table 3: G_∞, β and $\langle\tau\rangle$ of PE-1:4-0.2 after the first stress-relaxation experiment. Relative increment of the residual stress $\sigma_{r,2}/\sigma_{r,1}$ between the two stress-relaxation.

Temperature (°C)	G_∞	β	$\langle\tau\rangle$ (min)	$\sigma_{r,2} / \sigma_{r,1}$ (%)
170	0.06	0.35	1090	28
180	0.21	0.37	178	39
200	0.15	0.41	69	50
220	0.15	0.34	24	57

3.7 Shape memory properties.

Hartwig and co-workers have investigated the shape memory properties of thermoset/polycaprolactone networks incorporating crystallinity and exchangeable links [47]. The existence of chemical links between the crystallizable part and the network was found to partially decrease crystallinity but on the other hand to improve shape fixity and toughness [48]. The materials hereby investigated are networks wherein the crystallizable sequence is completely bound by chemical links. At room temperature, PE is well above the glass transition ($T_g \approx$ -120°C) and well below the melting point ($T_m \approx$ 106°C). Measurements of crystallinity by DSC are reported in SI (Fig. S4, Table S1). Since the areas of the melting peaks of crosslinked and non-crosslinked samples are of the same order, it is evident that crystallinity is to a large extend preserved after modification. The introduction of covalent bonds along the chains of the semi-crystalline polymer precursor creates a chemically crosslinked network in addition to the crystalline aggregation. Therefore, the synthesized

materials gather the structural features of a shape memory polymer being dually crosslinked by chemical links and physical links. The latter can be easily removed by heating above the melting point. Consequently, the shape memory behaviour of sample PE-1:4:0.2 was assessed in elongation under a cyclic stress of 100 kPa. The result of the shape memory sequence is presented in Fig. 6.

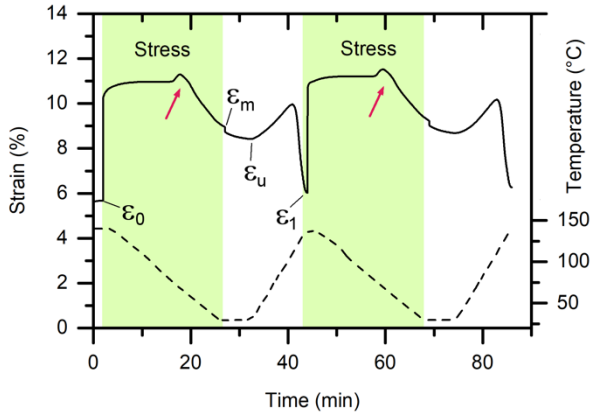

Fig. 6: Cyclic shape memory tests of compound PE-1:4-0.2 in tension mode. The green background areas indicate sections of 100 kPa applied stress. The represented variables are used in formulas 7 and 8, their meaning is explained in the text. The overshoots signaled by red arrows are discussed in Section 3.8.

As can be seen from the figure, the initial deformation of the sample is already ε_0 = 5.6% at rest. This deviation from zero might be ascribed to different factors, including the preload force (≈0.01 N) applied by the machine to hold the sample in tension. In parallel with this, between clamping at room temperature and equilibration at 140°C, the sample undergoes regular thermal expansion and volume change upon melting. While in this case the contribution of the preload tension (amounting to about 1 kPa) can be neglected, the other two can be estimated from tabulated volume-temperature diagrams of polyethylenes [49]. For a LDPE grade of similar density (0.92) [25] the linear expansion between these two temperatures is given by formula (7) :

$$\varepsilon_T = \sqrt[3]{\frac{v_{140}}{v_{30}}} - 1 \qquad (7)$$

where v_{140} and v_{30} are the specific volumes of polyethylene at 140 and 30°C; the values retained for calculation are 1.27 and 1.09, respectively. The result ε_T = 5.2% matches the experimental deviation at the beginning of the experiment. Thus the initial strain is attributable to thermal volume changes.

From this initial point, the sample is deformed by applying a constant stress of 100 kPa and then cooled to 30°C to freeze the deformation. During cooling, the shape of the sample

evolves in a non-monotonic way (Fig. 6) this point will be examined below. So far, the final strain, right before removing stress is noted ε_m. Then, after removing the stress, the sample is equilibrated at room temperature and the new strain attained at the end of the equilibration period is noted ε_u. During the last segment of the shape memory test, the sample is re-heated without external stress and its shape is recorded. The strain at the end of the first cycle is noted ε_1 (Fig. 6).

Using above definitions, the shape-fixity R_f and shape-recovery R_r performances may be determined in the usual way [26] according to equations (8) and (9):

$$R_f = \frac{\varepsilon_u}{\varepsilon_m} \cdot 100 \qquad (8)$$

$$R_r = \frac{\varepsilon_u - \varepsilon_1}{\varepsilon_m - \varepsilon_0} \cdot 100 \qquad (9)$$

The results for both cycles are reported in Table 4. From these raw numbers, the material apparently shows good fixity but modest recovery. However, the inconvenience of measuring in tension is that thermal contraction/expansion and the shape memory effects occur along the same axis. To disentangle the effects, one can use another geometry (e.g. flexion, torsion) where thermal expansion is intrinsically compensated. Another approach proposed here is to apply a correction of thermal expansion. In practical terms, this means replacing ε_1 and ε_0 (measured at 140°C) in formulas (8) and (9) by their corrected counterparts, ε_1-ε_T and ε_0-ε_T. With this correction (Table 4) the performance in shape recovery is close to 90%, while correction has no incidence on the shape fixity value.

Table 4: shape finixy R_f and shape recovery R_r of PE-1:4-0.2 at 140°C and 200°C for 2 different cycles.

Temperature	*First cycle (%)*		*Second cycle (%)*		
	R_f	R_r	R_f	R_r	
140°C	94	73	95	75	non-corrected
140°C	94	90	95	91	corrected

This demonstrates the efficiency of shape memory properties of these materials as well as the opportunity of applying the thermal expansion correction in this geometry.

In the following of this section, thermal correction will be considered to analyse the interplay between vitrimer properties and shape memory properties which become apparent when the

shaping stress is applied at a temperature high enough to activate the bond exchange reactions.

Shape memory experiments relevant to such conditions are presented in Fig. 7 where two different experiments at 140°C and 200°C are compared. The first step (Fig. 7a) corresponds to the shaping stage, which is essentially a regular isothermal creep test in response to a constant 100 kPa tensile stress. The stress duration is the same for both temperatures. In these plots, the deformation (draw ratio L/L_0) is determined relative to the length of the sample right before application of the stress (normalized to 1). Evidently, the deformation reached after one hour differs depending on whether the 100 kPa stress is applied at 140°C or 200°C. The excess creep observed at 200°C is the result of the plastic deformation of the network permitted by thermally activated bond exchange reactions.

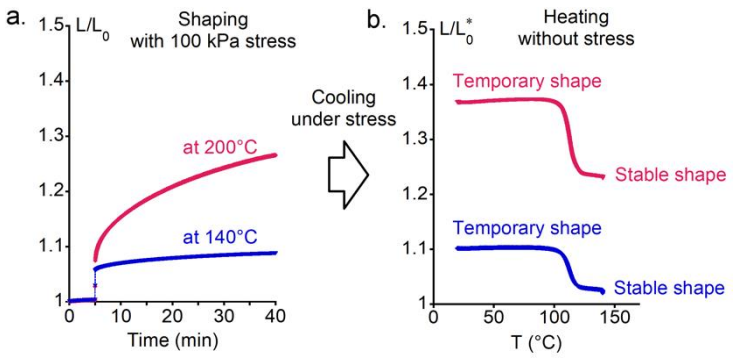

Fig. 7. thermomechanical cycles at 140 °C (blue curves) and 200°C (red curves) to assess shape memory behaviour and shape reconfiguration behaviour of PE-1:4:0.2;

The second stage of the experiment is a cooling ramp at -10°C/min and the peculiarities of this step will be presented at the end of the section; after cooling, the samples are ready for the strain recovery test. For the recovery stage, which is not isothermal, a real-time thermal correction is achieved the following way: the length of the sample at any time is divided by the length of a reference sample subjected to the same thermal cycle but using a 10 kPa stretching stress, value at which thermal expansion effects are larger than mechanical deformations. The corrected draw ratio (L/L_0*) presented in Fig. 7b is determined through formula (10).

$$\frac{L}{L_0^*} = \frac{L}{L^{\mathrm{Ref}}} \cdot \frac{L_0^{\mathrm{Ref}}}{L_0} \qquad (10)$$

Where L is the length of the sample at any time, L^{Ref} the length of the reference specimen at the same instant of the heating/cooling cycle and L_0 and L_0^{Ref} their respective initial lengths at 140°C. For the blue curve of Fig 7b (after shaping at 140°C), L/L_0* is of about 10% of the

starting length. This deformation almost completely vanishes after re-heating. In contrast for the red curve of Fig 7b (after shaping at 200°C under the same stress) L/L_0* is more than 35% and part of this deformation remains after reheating, meaning that the permanent (equilibrium) shape of the sample is >20% longer than the initial one. Thus after reshaping at 200°C, the sample still shows shape memory properties but the process starts from a new transient shape and ends with a new recovered shape. The sample deformation acquired at the end of this process is permanent and not recoverable by re-heating. This type of reconfiguration is characteristic of vitrimer materials; it is further illustrated qualitatively in the picture sequence of Fig. 8 where a ribbon shaped at 140° into a helicoïd completely recovers its initial flat shape during next heating whereas another sample twisted and held for enough long time at 200°C (1 hour in an oven) keeps the imprinted shape during further heating.

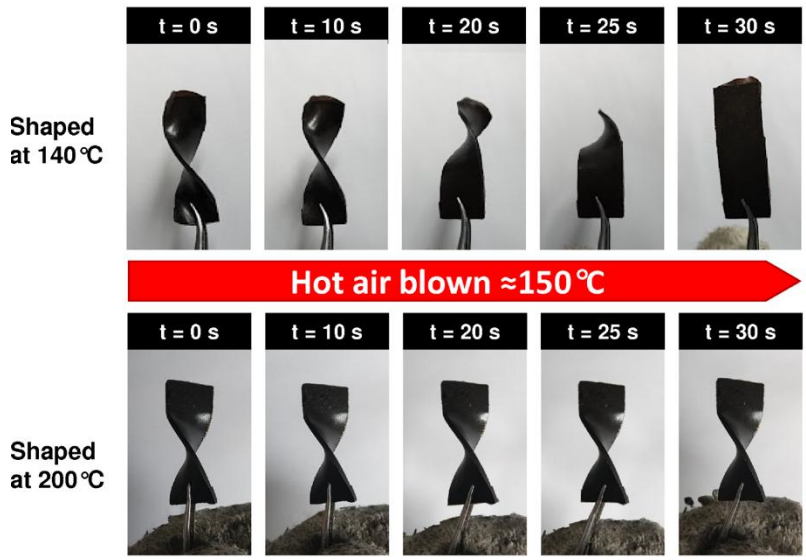

Fig. 8. Schematic illustration over 30 s of the double reconfiguration of PE-1:4-0.2 in two distinct conditions.

3.8 Strain induced crystallization.

In this section, we focus on another thermomechanical effect, observed with these samples. During a cooling ramp under constant tensile stress and constant cooling rate, the sample first elongates, then shrinks. This peculiarity is already visible and signaled by a red arrow on both cooling cycles shown in Fig. 6. It is further detected on the cooling ramps recorded at the end of the thermal cycles shown in Fig. 7. These cooling ramps are illustrated in Fig. 9, where the draw ratio L/L_{140}, relative to the initial length at 140°C is plotted together with the cooling ramp of the reference sample (stretched at 10 kPa instead of 100 kPa). The decreasing

portions of these plots, present for all samples, is simply attributable to specific volume changes upon cooling and crystallization. For samples stretched at 100 kPa, a distinctive increase of the sample length is also detected in the vicinity of the crystallization temperature.

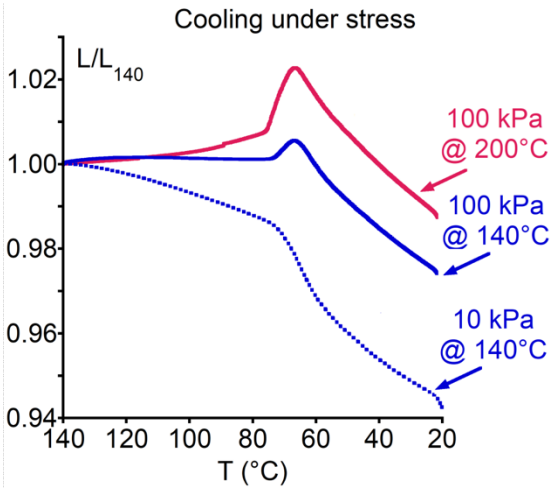

Fig. 9. Temperature variation of the draw ratio L/L_{140} during cooling under constant tensile stress.

In contrast, there is a continuous decrease of length for the reference sample. The increasing part of the curve therefore correlates with the simultaneous presence of stretching stress and crystallization. Similar effects have been reported in the literature and attributed to the oriented nucleation in stretched crosslinked polymers. This phenomenon sometimes referred to as "crystallization-induced elongation" is a consequence of the orientation of early-formed crystals in the direction of drawing, resulting in further anisotropization of the network [50]. This effect has been observed to be more evident for semi-crystalline networks with high gel content [51]. Interestingly, the phenomenon is amplified in the sample stretched at 200°C suggesting that network nodes in conflict with elongation may rearrange through exchange reactions, resulting in impoved anisotropy in the end.

4. Perspective

Production of the pre-vritrimer by continuous extrusion

The pre-vitrimer mixture of p(E-co-GMA) and dicarboxylate/dicarboxylic acid obtained upon extrusion is a thermolatent mixture that can react and form a network when heated at high enough temperature. Since the gap between the curing temperature and the melting point of the polymer precursor is sufficiently large, the pre-vitrimer can be kept at 115°C (temperature of extrusion and compression molding) without incurring gelation at too short times. This distinctive feature allowed us to convert a thermoplastic polymer into an elastic network in

batch extrusion. In the same way, upscaling the production of polyethylene-based vitrimers may be envisioned as the risk of cross-linking inside the extruder is controlled, which is here achieved through proper selection of composition, shear rate and temperature. In this perspective, a powdered mixture according to the PE-1:4:0.2 composition was introduced at the top feeder entrance of a continuous twin-screw vertical extruder. For this experiment, the temperature was regulated at 115°C all along the different portions of the screws, except for the last zone set at 125°C. The rotational speed of the screws was set on 70 rpm, corresponding to an overall residence time of ~3 min. Right after coming out of the column, the extruded filament slightly expanded and crystallized, resulting to production of a solid wire of about 2.7 mm diameter at a rate of about 15 mm/s eventually pelletized at the end of the extrusion line. We were able to extrude a total of 120 g of the *pre-vitrimer* mixture of PE-1:4:0.2 at an average rate of about 180 g/h. Pictures of extruded strands and pellets are presented in Fig. 10, their regular cylindrical shapes without corrugations strongly suggest that gelation is not attained.

Fig. 10. Samples of as-formed (left) and on-line pelletized (right) extruded filament of the PE-1:4:0.2 composition. At this stage, the compound is in its thermolatent pre-vitrimer form.

In the IR analysis (Fig. S8), the characteristic signal of epoxy groups is still present after extrusion. Based on the data presented in Fig. 3b the rise of viscosity takes place after 3 min at 170°C for this composition (dark blue plot). We believe that processing at such moderate extrusion rate is advisable to avoid internal overheating while preserving a large margin of latency for further processing and longer residence time in case of an incidental interruption of the process.

5. Conclusions

In this work, we show an example of polyolefin vitrimer where the percentage of chains not linked to the network is close to zero. In contrast to hitherto explored polyolefin vitrimers where networks featuring a large portion of soluble fraction were obtained by radical grafting of by blending a crosslinkable copolymer with a homopolymer, the current work addresses the use of ethylene copolymers for preparation of homogeneous networks. Considering a random copolymer with an average number of >400 monomers per chain and no more than 1 % of reactive comonomer, the statistical distribution analysis led to the conclusion that chains deprived of any reactive groups represent less than 6 wt% and experimentally a gel content up to 96 wt% was achieved. Nevertheless, such networks have been easily produced by batch and continuous extrusion processes, thanks to the latency of the epoxy-acid addition, which also avoids any release of water, gas or by products. The fully cured networks demonstrated stress relaxation with an activation energy of about 120 kJ/mol. In comparison with epoxidized natural rubber derivatives where the same cross-linking strategy was adopted [21,52] the reaction here did not require the use of one equivalent of amine but only a catalytic quantity. Increase of catalyst content above 20 mol% was found to slow down the addition reaction. The materials of the current work are semi-crystalline and show interesting shape memory properties. In particular, interplay of network's reconfiguration and the crystallization induced orientation under stress that might be exploited to design reversible two-way shape memory polymers especially considering that such properties are critically dependant of high gel content.

6. Acknowledgements

Paolo Edera is thanked for his help in torsion rheology. The research leading to these results has received funding from the VITRIMAT program of the European Union's Horizon 2020 research and innovation programme under the Marie Sklodowska-Curie Grant agreement No 860911, Eric Drockenmuller and Damien Montarnal are thanked for helpful discussions.

7. References

[1] Orr, C.A.; Adedeji, A.; Hirao, A.; Bates, F.; Macosko, C.W. Flow-induced reactive self-assembly. *Macromoelcules* **1997**, 30, 1243−1246.

[2] Pernot, H.; Baumert, M.; Court, F.; Leibler, L. Design and properties of co-continuous nanostructured polymers by reactive blending. *Nature Mater*. **2002**, *1* (1), 54-58. https://doi.org/10.1038/nmat711.

[3] Orr, C.A.; Cernohous, J.J.; Guegan, P.; Hirao, A.; Jeon, H.K.; Macosko, C.W. Homogeneous reactive coupling of terminally functional polymers. *Polymer* **2001**, *42*, 8171.

[4] Abbas, L.; Bouquey, M.; Flat, J.J.; Muller, R. New method for post-processing crosslinking reaction. *European Polymer Journal* **2008**, *44* 1238–1246.

[5] Montarnal, D.; Capelot, M.; Tournilhac, F.; Leibler, L. Silica-Like Malleable Materials from Permanent Organic Networks. *Science* **2011**, *334* (6058), 965–968.

[6] Demongeot, A.; Groote, R.; Goossens, H.; Hoeks, T.; Tournilhac, F.; Leibler, L. Cross-Linking of Poly(Butylene Terephthalate) by Reactive Extrusion Using Zn(II) Epoxy-Vitrimer Chemistry. *Macromolecules* **2017**, 50 (16), 6117–6127. https://doi.org/10.1021/acs.macromol.7b01141.

[7] Röttger, M.; Domenech, T.; Weegen, R. van der; Breuillac, A.; Nicolaÿ, R.; Leibler, L. High-Performance Vitrimers from Commodity Thermoplastics through Dioxaborolane Metathesis. *Science* **2017**, 356 (6333), 62–65.

[8] Kar, G.P.; Saed, M.A.; Terentjev, E.M. Scalable upcycling of thermoplastic polyolefins into vitrimers through transesterification. *J. Mater. Chem. A*, **2020**, 8, 24137.

[9] Montoya-Ospina, M.C.; Verhoogt, H.; Ordner, M.; Tan, X.; Osswald, T.A. Effect of cross-linking on the mechanical properties, degree of crystallinity and thermal stability of polyethylene vitrimers. *Polym. Eng. Sci.* **2022**, 62, 4203–4213. https://doi.org/10.1002/pen.26178.

[10] Saed, M. O.; Lin, X.; Terentjev, E. M. Dynamic Semicrystalline Networks of Polypropylene with Thiol-Anhydride Exchangeable Crosslinks. *ACS Appl. Mater. Interfaces* **2021**, *13* (35), 42044–42051. https://doi.org/10.1021/acsami.1c12099.

[11] Fenimore, L.M.; Chen, B.; Torkelson, J.M. Simple Upcycling of Virgin and Waste Polyethylene into Covalent Adaptable Networks: Catalyst-Free, Radical-Based Reactive Processing with Dialkylamino Disulfide Bonds. *J. Mater. Chem. A* **2022**, 10, 24726–24745. https://doi.org/10.1039/D2TA06364F.

[12] Ricarte, R.G.; Tournilhac, F.; Cloître, M.; Leibler, L. Linear Viscoelasticity and Flow of Self-Assembled Vitrimers : The Case of a Polyethylene / Dioxaborolane System. *Macromolecules*, **2020**, 53, 1852, DOI:10.1021/acs.macromol.9b02415

[13] Farge, L.; Hoppe, S.; Daujat, V.; Tournilhac, F.; André, S. Solid Rheological Properties of PBT Based Vitrimers. *Macromolecules* **2021**, 54 (4), 1838–1849. https://doi.org/10.1021/acs.macromol.0c02105.

[14] Canadell, J.; Goossens, H.; Klumperman, B. Self-Healing Materials Based on Disulfide Links. *Macromolecules* **2011**, 44, 2536–2541. https://doi.org/10.1021/ma2001492

[15] Lafont, U.; van Zeijl, H.; Van der Zwaag, S. Influence of Cross-linkers on the Cohesive and Adhesive Self-Healing Ability of Polysulfide-Based Thermosets. *ACS Appl. Mater. Interfaces* **2012**, 4, 6280−6288. https://doi.org/10.1021/am301879z

[16] Rekondo, A.; Martin, R.; Luzuriaga, A. R. de; Cabañero, G.; Grande, H. J.; Odriozola, I. Catalyst-Free Room-Temperature Self-Healing Elastomers Based on Aromatic Disulfide Metathesis. *Mater. Horiz.* **2014**, 1 (2), 237–240. https://doi.org/10.1039/C3MH00061C.

[17] Ruiz de Luzuriaga, A.; Martin, R.; Markaide, N.; Rekondo, A.; Cabañero, G.; Rodriguez, J.; Odriozola, I. Epoxy resin with exchangeable disulfide crosslinks to obtain reprocessable, repairable and recyclable fiber-reinforced thermoset composites. *Mater. Horiz.*, **2016**, 3, 241-247. https://doi.org/10.1039/C6MH00029K

[18] Guggari, S.; Magliozzi, F.; Malburet, S.; Graillot, A.; Destarac, M.; Guerre, M. Vanillin-Based Epoxy Vitrimers: Looking at the Cystamine Hardener from a Different Perspective. *ACS Sus. Chem. Eng.* **2023**, 11, 6021-6031. https://doi.org/10.1021/acssuschemeng.3c00379.

[19] Otsuka, H.; Nagano, S.; Kobashi, Y.; Maeda, T.; Takahara, A. A Dynamic Covalent Polymer Driven by Disulfide Metathesis under Photoirradiation. *Chem. Commun.* **2010**, 46, 1150–1152. https://doi.org/10.1039/B916128G.

[20] Ainavarapu, S.R.K.; Wiita, A.P.; Dougan, L.; Uggerud, E.; Fernandez, J.M. Single-Molecule Force Spectroscopy Measurements of Bond Elongation during a Bimolecular Reaction. *J. Am. Chem. Soc.* **2008**, 130, 6479–6487. https://doi.org/10.1021/ja800180u.

[21] Imbernon, L.; Oikonomou, E.K.; Norvez, S.; Leibler, L. Chemically Crosslinked yet Reprocessable Epoxidized Natural Rubber via Thermo-Activated Disulfide Rearrangements. *Polym. Chem.* **2015**, 6 (23), 4271–4278. https://doi.org/10.1039/C5PY00459D.

[22] Chen, M.; Zhou, L.; Wu, Y.; Zhao, X.; Zhang, Y. Rapid Stress Relaxation and Moderate Temperature of Malleability Enabled by the Synergy of Disulfide Metathesis and Carboxylate Transesterification in Epoxy Vitrimers. *ACS Macro Letters* **2019**, 8 , 255–260. https://doi.org/10.1021/acsmacrolett.9b00015.

[23] Capelot, M.; Unterlass, M. M.; Tournilhac, F.; Leibler, L. Catalytic Control of the Vitrimer Glass Transition. ACS Macro Lett. 2012, 1 (7), 789–792. https://doi.org/10.1021/mz300239f

[24] Yamawake, K.; Hayashi, M.; The role of tertiary amines as internal catalysts for disulfide exchange in covalent adaptable networks. *Polym. Chem.* **2023**, 14, 680-686. https://doi-org.inc.bib.cnrs.fr/10.1039/D2PY01406H

[25] Capt, L.; Kamal, M. R. The Pressure-Volume-Temperature Behavior Polyethylene Melts. *Intern. Polymer Processing* **2000**, 15, 83.

[26] Lendlein, A.; Kelch, S. Shape-Memory Polymers. *Angewandte Chemie International Edition* **2002**, 41, 2034–2057. https://doi.org/10.1002/1521-3773(20020617)41:12<2034::AID-ANIE2034>3.0.CO;2-M

[27] Reano, A. F.; Guinault, A.; Richaud, E.; Fayolle, B. Polyethylene loss of ductility during oxidation: Effect of initial molar mass distribution. *Polym. Degr. Stab.* **2018**, *149*, 78–84.

[28] Ricarte, R. G.; Tournilhac, F.; Leibler, L. Phase Separation and Self-Assembly in Vitrimers: Hierarchical Morphology of Molten and Semicrystalline Polyethylene/Dioxaborolane Maleimide Systems. *Macromolecules* **2019**, *52* (2), 432–443.

[29] May, C. *Epoxy Resins: Chemistry and Technology, Second Edition,*Marcel Dekker, New York 1988.

[30] Pratt, R. C.; Lohmeijer, B. G. G.; Long, D. A.; Waymouth, R. M.; Hedrick, J. L. Triazabicyclodecene: A Simple Bifunctional Organocatalyst for Acyl Transfer and Ring-Opening Polymerization of Cyclic Esters. *J. Am. Chem. Soc.* **2006**, 128, 4556–4557. https://doi.org/10.1021/ja060662+

[31] Poutrel, Q.A.; Blaker, J.J.; Soutis, C.; Tournilhac, F.; Gresil, M. Dicarboxylic acid-epoxy vitrimers: influence of the off-stoichiometric acid content on cure reactions and thermo-mechanical properties. *Polym. Chem.*, **2020**, 11, 5327. https://doi.org/10.1039/d0py00342e.

[32] Tanaka, Y. Catalytic Effects of Substituted Pyridines and Quinolines on the Reaction of Phenyl Glycidyl Ether and Benzoic Acid. *J. Org. Chem.* **1967**, *32* (8), 2405–2409. https://doi.org/10.1021/jo01283a010.

[33] Tanaka, Y.; Takeuchi, H. Dielectric and Hydrogen-Bonding Effects of Solvents on the Base-Catalysed Reaction of Phenyl Glycidyl Ether with Benzoic Acid. *Tetrahedron* **1968**, *24* (21), 6433–6448. https://doi.org/10.1016/S0040-4020(01)96835-8.

[34] Popli, R.; Glotin, M.; Mandelkern, L.; Benson, R. S. Dynamic Mechanical Studies of α and β Relaxations of Polyethylenes. *Journal of Polymer Science: Polymer Physics Edition* **1984**, *22* (3), 407–448. https://doi.org/10.1002/pol.1984.180220306.

[35] Lei, Z.Q.; Xiang, H.P.; Yuan, Y.J.; Rong M.Z., Zhang, M.Q. Room-Temperature Self-Healable and Remoldable Cross-linked Polymer Based on the Dynamic Exchange of Disulfide Bonds. *Chem. Mater.* **2014**, 26, 2038–2046. http://doi.org/10.1021/cm4040616

[36] Humphrey, R. E.; Hawkins, J. M. Reduction of Aromatic Disulfides with Triphenylphosphine. *Anal. Chem.* **1964**, 36, 1812–1814. https://doi.org/10.1021/ac60215a035

[37] Cleland, W. W. Dithiothreitol, a New Protective Reagent for SH Groups*. *Biochemistry* **1964**, 3, 480–482. https://doi.org/10.1021/bi00892a002.

[38] Koval', I. V. The Chemistry of Disulfides. Russ. Chem. Rev. **1994**, 63, 735–750. https://doi.org/10.1070/RC1994v063n09ABEH000115.

[39] Kandemir, D.; Luleburgaz, S.; Gunay, U. S.; Durmaz, H.; Kumbaraci, V. Ultrafast Poly(Disulfide) Synthesis in the Presence of Organocatalysts. *Macromolecules* **2022**, *55* (17), 7806–7816. https://doi.org/10.1021/acs.macromol.2c01228.

[40] Nevejans, S.; Ballard, N.; Miranda, J. I.; Reck, B.; Asua, J. M. The Underlying Mechanisms for Self-Healing of Poly(Disulfide)s. *Phys. Chem. Chem. Phys.* **2016**, *18* (39), 27577–27583. https://doi.org/10.1039/C6CP04028D.

[41] Pepels, M.; Filot, I.; Klumperman, B.; Goossens, H. Self-Healing Systems Based on Disulfide–Thiol Exchange Reactions. *Polym. Chem.* **2013**, 4, 4955–4965. https://doi.org/10.1039/C3PY00087G.

[42] Bach, R. D.; Dmitrenko, O.; Thorpe, C. Mechanism of Thiolate−Disulfide Interchange Reactions in Biochemistry. *J. Org. Chem.* **2008**, 73, 12–21. https://doi.org/10.1021/jo702051f.

[43] Matxain, J. M.; Asua, J. M.; Ruipérez, F. Design of New Disulfide-Based Organic Compounds for the Improvement of Self-Healing Materials. *Phys. Chem. Chem. Phys.* **2016**, 18, 1758–1770. https://doi.org/10.1039/C5CP06660C.

[44] Ma, Z.; Wang, Y.; Zhu, J.; Yu, J.; Hu, Z. Bio-Based EpoxyVitrimers: Reprocessibility, Controllable Shape Memory, and Degradability. *J. Polym. Sci., Part A: Polym. Chem*. **2017**, 55(10), 1790−1799

[45] Ruiz de Luzuriaga, A.; Azcarate-Ascasua, I.; Boucher, V.; Solera, G.; Grande, H. J.; Rekondo, A. Chemical control of the aromatic disulfide exchange kinetics for tailor-made epoxy vitrimers. *Polymer* **2022**, 239, 124457

[46] Schenk, V.; D'Elia, R.; Olivier, P.; Labastie, K.; Destarac, M.; Guerre, M. Exploring the Limits of High-Tg Epoxy Vitrimers Produced through Resin-Transfer Molding *ACS Appl. Mater. Interfaces* **2023**, 15, 46357–46367. https://doi.org/10.1021/acsami.3c10007

[47] Arnebold, A.; Wellmann, S.; Hartwig, A. Network dynamics in cationically polymerized, crosslinked epoxy resins and its influence on crystallinity and toughness. *Polymer* **2016**, 91, 14−23. http://dx.doi.org/10.1016/j.polymer.2016.03.052

[48] Schäfer, A, Hartwig, A.; Koschek, K. The nature of bonding matters: Benzoxazine based shape memory polymers. *Polymer* **2018**, 135, 285−294. https://doi.org/10.1016/j.polymer.2017.12.029

[49] Mandelkern, L. The Melting of Crystalline Polymers. *Rubber Chem. Technol.* **1959**, 32, 1392.

[50] Chung, T.; Romo-Uribe, A.; Mather, P. T. Two-Way Reversible Shape Memory in a Semicrystalline Network. *Macromolecules* **2008**, 41, 184–192. https://doi.org/10.1021/ma071517z

[51] Huang, M.; Dong, X.; Wang, L.; Zhao, J.; Liu, G.; Wang, D. Two-Way Shape Memory Property and Its Structural Origin of Cross-Linked Poly(ε-Caprolactone). *RSC Adv.* **2014**, 4, 55483–55494. https://doi.org/10.1039/C4RA09385B

[52] Imbernon, L.; Norvez, S.; Leibler, L. Stress Relaxation and Self-Adhesion of Rubbers with Exchangeable Links. *Macromolecules* **2016**, 49, 2172−2178. http://10.1021/acs.macromol.5b02751